



Adsorption removal of nitrate by a novel magnetic zeolite adsorbent (zeolite/ γ -Fe₂O₃ nanocomposite) in solution

Esmael Darezereshki¹ · Fereshteh Bakhtiari² · Mehri Rahmani²

Received: 18 February 2022 / Accepted: 25 September 2022 / Published online: 15 October 2022
© The Author(s), under exclusive licence to Springer Nature Switzerland AG 2022

Abstract

Due to the presence of nitrate ions in various sources, including industrial and domestic water, the aim of the present research was to remove nitrate ions from aqueous solution using a new adsorbent of zeolite modified with maghemite (γ -Fe₂O₃) nanoparticles. The maximum nitrate removal capacities of the as-prepared adsorbents in solution were investigated against influencing factors like shaking time, adsorbent dose, temperature, solution pH and initial nitrate concentration. The adsorption–desorption interaction of the zeolite/gamma Fe₂O₃ nanocomposite with the adsorbate was also investigated. Several instrumental techniques such as XRD, BET, FTIR, SEM and TEM analysis were utilized to examine the adsorption mechanisms like ion exchange, complexation and electrostatic interactions. Results indicated that in comparison with the other adsorbents used for nitrate removal, the present adsorbent exhibits high adsorption capacity (421.5 mg/g) in a shorter time (5 min) with adsorbent dosage of 0.2 g/L at room temperature. The highest removal of nitrate was 91.5% at initial nitrate concentration of 100 mg/L, adsorbent dosage of 2 g/L and pH=6. The adsorption process followed the Langmuir model and pseudo-second-order kinetics. It was also found that after three times of adsorbent (magnetic zeolite) regeneration by H₂O₂, the removal percentage was still more than 85.

Keywords Adsorption · Magnetic · Nanocomposite · Nitrate · Zeolite

Introduction

The fast growth in city life and agricultural activities has led to one of the most important problems of the twenty-first century, which is the pollution of water resources. Among different inorganic contaminants, nitrogen-containing compounds such as ammonium (NH₄⁺), ammonia (NH₃), nitrate (NO₃⁻) and nitrite (NO₂⁻) are real hazards to the environment and health [1]. Biological and chemical processes can

oxidize nitrite to nitrate or reduce it to various compounds [2]. The nitrate is the stable form of nitrogen (N) as pollutants in the environment and water supplies [2, 3]. The nitrate converted into nitrite in water could cause vital health risks when it contacts hemoglobin [4]. In humans, the excess amount of nitrate and nitrite may cause kidney failure, cancer, blue-baby syndrome, especially infectious diseases, Alzheimer's disease, the potential formation of carcinogenic nitrosamines, etc. [1, 2, 5]. The allowable concentration of nitrate in drinking water by the World Health Organization (WHO) is 40–50 mg/L [1, 6–8]. In addition, an epidemiological investigation has showed that long time usage of drinking water with 18 mg/L NO₃ could lead to non-Hodgkin's lymphoma (NHL) [5]. Nitrate ions are present in the primary and secondary wastewater sources like industrial wastes, sewage sludge, household wastes and surface water [6]. Tasks such as excess use of nitrogenous fertilizers, discharge of industrial production of glass, explosives, discharges from various chemical production and separation processes, biological waste decomposition such as disposal of untreated sanitary, leakage from septic systems, landfill leachate, and animal manure lead to release of nitrate ions

✉ Esmael Darezereshki
Darezereshki@uk.ac.ir

Fereshteh Bakhtiari
Fereshteh@uk.ac.ir

Mehri Rahmani
Dz.esmaeel@gmail.com

¹ Department of Materials Engineering, Shahid Bahonar University of Kerman, Engineering Faculty, P.O. Box 76169-133, Kerman, Iran

² Faculty of Engineering, Department of Chemical Engineering, Shahid Bahonar University of Kerman, P.O. Box 76169-133, Kerman, Iran

into the environment and water sources [1, 2, 8]. For the purpose of eliminating the nitrogen-containing pollutants from water and waste water resources, recently several methods have been used, such as bio and chemical denitrification [8, 9], ion exchange [5, 8, 10–13], catalytic reduction [8, 14–16], reverse osmosis [2, 8], and adsorption [1, 3, 4, 6, 7, 10, 17–24]. Among the various technologies, the adsorption technique is presented as the most effective method in a wide range of applications leading to eco-friendly, high safety, simple and fast processes with economic benefits [1, 6]. Moreover, it does not cause the formation of any secondary pollutants [6].

Due to the relatively low cost of natural and green materials [25], different kinds of natural adsorbents such as zeolite [26], herschelite-sodium chabazite [1], bentonite [1], clays [27], metal oxide [4] and chitosan [4] have been used for the removal of nitrate contaminants from aqueous solutions [1]. Because of the potential of adsorption ions with positive charge, zeolites are very popular for adsorbing small cations like nitrate and metal ions. Nevertheless, when raw zeolite particles are dissolved in a solution, because of their net negative surface charge, they have a little affinity for adsorbing anions which means they are not suitable for the removal of anionic contaminants. With the aim of modifying zeolites' surface properties and enhancing removal of anionic water pollutants, the zeolites are treated by HCl and modified by maghemite nanoparticles [21]. Nanotechnology can improve and make the above-mentioned conventional techniques more effective for environmental applications such as water, soil treatment, and pollutant separation [7, 28]. The most important factor in the adsorption procedure is to choose a suitable adsorbent substance, which can adsorb dissolved contaminants on the surface and then easily release it [1]. Application of advanced technology such as nanomaterials has some advantages like self-assembly, large surface area and enhanced reactivity reported in the literature [14, 22, 28, 29]. These reports have shown the advantages of magnetically modified materials to be ease of separation and high adsorption efficiency. Hence, the magnetically modified natural materials have recently received significant attention in the water purification research field [2, 6, 14, 15, 17, 24, 30, 31]. A few articles are attributed to the provision of magnetic carbon substances (such as zinc ferrite-activated carbon [6], magnetic MWCNTs (multi-walled carbon nanotubes) [17]), and these materials were utilized for the elimination of dyes, toxic cations, anions and other organic contaminants from aqueous solutions. The magnetic nanoparticles studied thus far focus on their influence as an appropriate adsorbent for nitrate removal from water because of their high specific surface area, non-toxicity, easy separation by a magnet, rapid response, and high efficiency [17].

Adsorption with cheap sorbents such as zeolite is a cost-effective way for the removal of nitrate. Due to the

abundance of clinoptilolite zeolite mines in Iran and its very low price and high efficiency in removal of the ions such as ammonium and nitrate, it seems to be beneficial to use this adsorbent in treatment of the polluted water sources. The main problem of using natural zeolites such as clinoptilolite, however, is smallness of the pores of this adsorbent that limits catalytic adsorption of the nitrate. Therefore, modified clinoptilolite zeolite may accelerate adsorption rate and obtain higher efficiency of nitrate removal. The aim of the present research was to assess whether removal of nitrate ions from aqueous solution at high concentrations by a new adsorbent of zeolite/ γ - Fe_2O_3 nanocomposite will yield higher adsorption capacity and lower residence time compared to those reported by other researchers.

After preparing the nanocomposite adsorbents by a one-step chemical precipitation method, the morphology, crystal structure, functional group, specific surface area, and magnetic force of the prepared adsorbents were evaluated through several instrumental techniques such as X-ray diffraction (XRD), Brunauer–Emmett–Teller (BET), Fourier-transform infrared (FT-IR), scanning electron microscopy (SEM) and transmission electron microscopy (TEM). The adsorption performance of zeolite/gamma Fe_2O_3 nanocomposite was examined using the batch mode of adsorption.

Experimental

Materials

Zeolite/ γ - Fe_2O_3 nanocomposite was synthesized using stock aqueous solutions of chloride irons ($\text{FeCl}_3 \cdot 6\text{H}_2\text{O}$, $\text{FeCl}_2 \cdot 4\text{H}_2\text{O}$), natural zeolite powder (clinoptilolite) with the average particle size of 75 micron (Negin-Powder company of Semnan, Iran), ammonium hydroxide (25–30%, NH_4OH), hydrochloric acid (HCl, 37%) and ethanol ($\text{CH}_3\text{CH}_2\text{OH}$, 99.93%). Potassium nitrate salt (KNO_3) supplied by Merck Company was the basis to prepare nitrate materials required in adsorption tests. Hydrochloric acid and sodium hydroxide solutions 0.1 M were used to set the pH of solutions. All other used chemicals were of analytical grade.

Preparation of treated zeolite

To determine the chemical elements of powder zeolite which was used in this study, X-ray fluorescence (XRF) analysis was done. To obtain treated zeolite (TZ), 70 g of zeolite powder was impregnated in 500 mL of 4 M HCl and refluxed for 3 h at 50 °C. The product was separated by filtration and dried at 55 °C temperature. The surface area and the

water-holding capacity (WHC%) of the TZ were measured by BET and Keen cup method, respectively.

Synthesis of magnetic zeolite nanocomposite (zeolite/ γ -Fe₂O₃) by precipitation method

In a typical experiment of synthesizing zeolite/ γ -Fe₂O₃ nanocomposite by the precipitation method, 10 g of TZ was mixed with 150 mL solution of 1 M FeCl₃·6H₂O and 37.5 mL of 2 M FeCl₂·2H₂O (to keep the Fe³⁺/Fe²⁺ = 2). The mixed solution was mechanically stirred at 900 rpm, which was immersed in a room temperature (25 °C) water bath. The 400 mL of NH₃·H₂O solution (3 M) was dropped to these solutions. After ending the reaction (pH = 9.5), the dropping was stopped, the dark brown precipitate of magnetic zeolite (MZ) nanocomposite was collected by a manual magnet, washed several times with ethanol, and dried at 55 °C after filtration.

Treated zeolite and magnetic zeolite nanocomposite characterization

The structure of the TZ and MZ nanocomposite was identified by XRD (X'pert-MPD Philips equipped with a detector using CuK α radiation). To identify functional groups in the samples, FT-IR spectra of the TZ and MZ nanocomposite were recorded on a Bruker Tensor 27 instrument with an RT-DLATGS detector in the range 400–4000 cm⁻¹. To show the morphology of the TZ and MZ nanocomposite SEM (MIRA3-Tescan) was used, and TEM (Philips CM20) technique was utilized to determine the size of Fe₃O₄ nanoparticles on the MZ nanocomposite. To determine the specific surface area of the samples, BET measurements of N₂ adsorption were carried out at 77 K using an ASAP2020 instrument. V_{tot} was evaluated by converting the volume of nitrogen adsorbed at $p/p_s \approx 0.99$ to the volume of liquid adsorbate. Mass magnetization of the MZ nanocomposite versus the applied magnetic field was measured at room temperature for 120 min using a vibrating sample magnetometer (PAR-VSM 155R).

To obtain pH_{ZPC} (zero-point charge) of MZ, 0.5 g of nanocomposite was mixed with 100 mL solution of 0.01 M NaCl in nine different polyethylene vessels, and the pH set from 2 to 10 by 0.1 M HCl and NaOH in each vessel [32–37]. The nine vessels were then placed in a shaker incubator at 25 °C for 24 h. Finally, the zero-point charge of the adsorbent was estimated by drawing the difference in initial pH and the final pH ($\Delta\text{pH}_{\text{final}} - \Delta\text{pH}_{\text{initial}}$) against initial pH [32]. The pH of the solutions was measured by an 827-pH lab pH-meter (Metrohm).

Nitrate Adsorption Batch Tests

To investigate the effect of pH on the nitrate adsorption with MZ nanocomposite, one liter of nitrate ion solution (100 mg/L) was prepared by dissolving 100 mg KNO₃ in one-liter distilled water. Then, 100 mL of the nitrate solution was poured into each eight 250 mL of Erlenmeyer flasks, and pH set between 2–9 by 0.1 M HCl and NaOH. Into each container was added 0.02 g (0.2 g/L) of nanocomposite, and all of them were placed in a shaker incubator with 150 rpm at 25 °C for 48 h. After adsorption process, a magnet was used to manually remove the nanocomposite from solution. The solution was passed through a 0.22- μm syringe filter to ensure the validity of the separation procedure. Two milliliters of the solution were then subjected to nitrate concentration analysis using spectrophotometry (Model Optizen 3220).

The concentration of NO₃ before and after adsorption was measured by a spectrophotometer. The detection limit was 0.05 mg/L, and the relative standard deviation of five replicate analyses was generally below 2.5%. To determine the concentration of nitrate in the solution, at first 7 samples of standard solution were prepared with concentrations of 0 to 11 mg/L, and the adsorption amounts of each sample were measured by the spectrophotometer in wavelengths of 220 and 275 nm, followed by subtracting the double absorbance at 275 nm from the absorbance at 220 nm (Eq. 1). Then, by using these results to read the adsorption amounts of unknown samples and comparing to the standard curve of known nitrate concentration, the nitrate concentration of the samples was calculated from the calibration curve [38].

$$\text{Absorbance of nitrate} = \text{adsorption in 220 nm} - 2 * (\text{adsorption in 275 nm}) \quad (1)$$

To study the kinetics of nitrate removal, approximate concentrations of 100, 250 and 400 mg/L nitrate ions were used at initial pH of 6 and 25 °C. Then, 0.02 g of adsorbent was added to 100 mL of solution (0.2 g/L) and the residual nitrate concentration in the solution was measured at time intervals 1, 3, 5, 20, 30 and 60 min. Each test was performed in duplicate, and average values were recorded. In the control test, no change in initial nitrate concentration was observed without the presence of adsorbent at pH = 6. The experiments with TZ in the same conditions at 100 mg/L nitrate were performed to compare the adsorption kinetics with MZ nanocomposite.

Thermodynamic parameters such as ΔH° , ΔS° and ΔG° are obtained by the linearized Van't Hoff function and Gibbs free energy equations (Eqs. 2–4) [32]. ΔH° and ΔS° values are achieved by plotting the linear $\text{Ln}K_d$ diagram against $1/T$ and then extracting the slope and y-intercept of the aforementioned linear equation, respectively.

$$K_d = \frac{q_e}{C_e} \quad (2)$$

$$\Delta G^0 = \Delta H^0 - T\Delta S^0 \quad (3)$$

$$\ln K_d = -\frac{\Delta H^0}{R \cdot T} + \frac{\Delta S^0}{R} \quad (4)$$

where K_d is the adsorption distribution coefficient, q_e is the equilibrium concentration of nitrate on the adsorbent (mg/L), R is universal gas constant (8.314 J/mol K) and T is the absolute temperature in Kelvin [32].

For the thermodynamic study, the tests were done at initial pH=6, concentration of 100 mg/L nitrate, time of 5 min and 0.2 g/L of adsorbent in an incubator shaker with three different temperatures of 25, 35 and 45 °C.

To determine the nitrate adsorption isotherm, 0.02 g of adsorbent was added to 100 mL of solution with initial concentrations of 100, 250 and 400 mg/L. The initial pH of the solution was set to 7. The mixture of solution and adsorbent was stirred until equilibrium (120 min) in an incubator shaker at 150 rpm, and then, separation by hand magnet was done. Before measuring NO_3^- concentration by spectrophotometry, the solutions were passed through a 0.22-micron syringe filter.

The most widely accepted surface adsorption isotherm models for single solute systems are by Langmuir and Freundlich [32–37]. The obtained adsorption amount and the concentration of the liquid phase were tested with them. Linear regression is often used to determine the best-fitting isotherm, and the applicability of isothermal equations is compared by judging the correlation coefficients.

The Langmuir equation is commonly expressed as follows (Eq. 5) [32–37]:

$$C_e/q_e = (1/K_L q_m) + (1/q_m) C_e \quad (5)$$

where q_m is monolayer adsorption capacity (mg/g), and K_L is Langmuir isotherm constant related to the affinity of the binding sites and energy of adsorption (L/mg). The values of q_m and K_L can be calculated by plotting C_e/q_e versus C_e .

The Freundlich equation was employed for the adsorption of nitrate on the adsorbent. The Freundlich isotherm is represented by Eq. (6) [32–37]:

$$\log q_e = \log K_f + 1/n \log C_e \quad (6)$$

where q_e is the amount of nitrate adsorbed (mg/g), C_e is the equilibrium concentration of nitrate in solution (mg/L), and K_f and n are constants incorporating the factors affecting the adsorption capacity and intensity of adsorption, respectively [32–37].

The kinetics of nitrate adsorption onto MZ nanocomposite is required for selecting optimum operating

conditions for the full-scale batch process. The kinetic parameters that are helpful for the prediction of adsorption rate give important information for designing and modeling the adsorption processes. Various kinetic models have been suggested to investigate the mechanism of adsorption. The two kinetic models used to better analyze the kinetics of nitrate adsorption by MZ nanocomposite are pseudo-first-order and pseudo-second-order.

The kinetic data were treated with the following Lagergren pseudo-first-order rate equation (Eq. 7) [32–37]:

$$\log(q_e - q_t) = \log q_e - k_f t/2.303 \quad (7)$$

where q_t and q_e are the amounts adsorbed at time t and at equilibrium (mg/g), and k_f is the pseudo-first-order rate constant for the adsorption process (min^{-1}).

Pseudo-second-order kinetic model (Eq. 8) [32–34]:

$$\frac{t}{q_t} = \frac{1}{k_2 q_e^2} + \frac{1}{q_e} t \quad (8)$$

where q_t (mg/g) is the adsorbed amount at time t , q_e (mg/g) is the maximum adsorption capacity, and k_2 (g/mg min) is the rate constant [32–34]. The pseudo-second-order kinetic model assumes chemisorption to be the rate-limiting step due to its tendency to involve electron exchange between the adsorbent and adsorbate [32–34].

Different amounts of adsorbent with concentrations of 0.2, 0.5, 1.5 and 2 g/L were used to evaluate the optimum amount of adsorbent in nitrate removal. For this purpose, 100 mL of nitrate solution with a concentration of 100 mg/L was prepared and certain amounts of adsorbent were added into each of the Erlenmeyer flasks. Test conditions were performed at ambient temperature, pH=6 and 150 rpm inside the incubator shaker with a residence time of 120 min.

Regeneration and reuse

First, 500 mL of nitrate solution with a concentration of 100 mg/L was prepared for the adsorption and desorption process. Three consecutive adsorption–desorption cycles were performed in duplicate to evaluate the feasibility of regenerating and reusing the MZ nanocomposite (zeolite/ γ - Fe_2O_3) adsorbent. The adsorption experiments were performed in 100 mL of solution with an initial concentration of 100 mg/L nitrate, pH=6 and an adsorbent of 2 g/L for 5 min. Thereafter, the magnetically separated MZ nanocomposite was gently and repeatedly rinsed with deionized water, followed by redispersion in 20 mL of regenerant, i.e., 0.2 mol/L H_2O_2 and HCl solution, and shaken for another 120 min. Before the next adsorption process, the MZ nanocomposite was washed with deionized water. After separation by hand

magnet, 100 mL of initial nitrate solution was added to it and the pH of the solution was adjusted to 6 with 0.01 M hydrochloric acid. These adsorption–desorption cycles were repeated three times, and the nitrate adsorption removal was analyzed and recorded.

Results and discussion

The characterization of nanocomposite

The XRF analysis of powder zeolite, which has been used in this study, showed that it contains 67% SiO₂, 12% Al₂O₃, 2% Na₂O, 2% K₂O, 1% CaO, 0.56% MgO and 0.52% Fe₂O₃. The BET surface area and WHC% of zeolite after treatment were 155 m²/g and 65%, respectively.

Figure 1 shows the XRD spectrum of the TZ (a) and MZ nanocomposite (b) obtained by the precipitation method. The presence of well-ordered and dispersed crystalline maghemite (γ -Fe₂O₃) is evident with lattice parameters: $a = 0.835$ nm, $b = 0.835$ nm, $c = 0.835$ nm on the TZ surface via chemical linking. All peaks in the XRD pattern are consistent with the standard structure (ICDD Card No. 39–1346) [39, 40], and the weak peaks appearing at $2\theta = 22^\circ$ and 27° correspond to the TZ [41]. The mean particle size of maghemite nanoparticles was estimated to be approximately 18 nm according to the Debye–Scherrer equation $D = (K\lambda)/(\beta \cdot \cos\theta)$, where λ is the wavelength of the X-ray used for the diffraction, K is a constant called shape factor ($K = 0.89$), θ is peak position ($2\theta/2$) in radians, and β is the full width at half-maximum (FWHM) intensity in radians [42–47].

Fig. 1 X-ray diffraction patterns of **a** TZ and **b** MZ

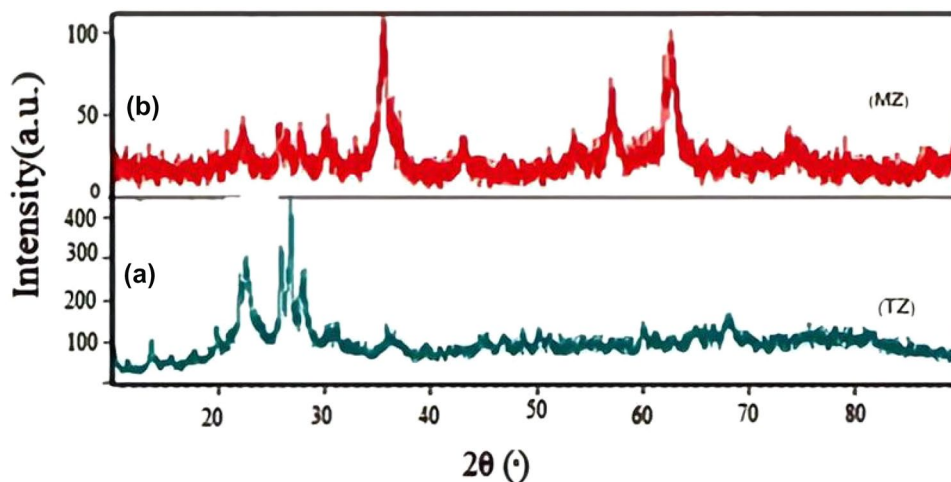


Fig. 2 FTIR spectra of **a** TZ and **b** MZ

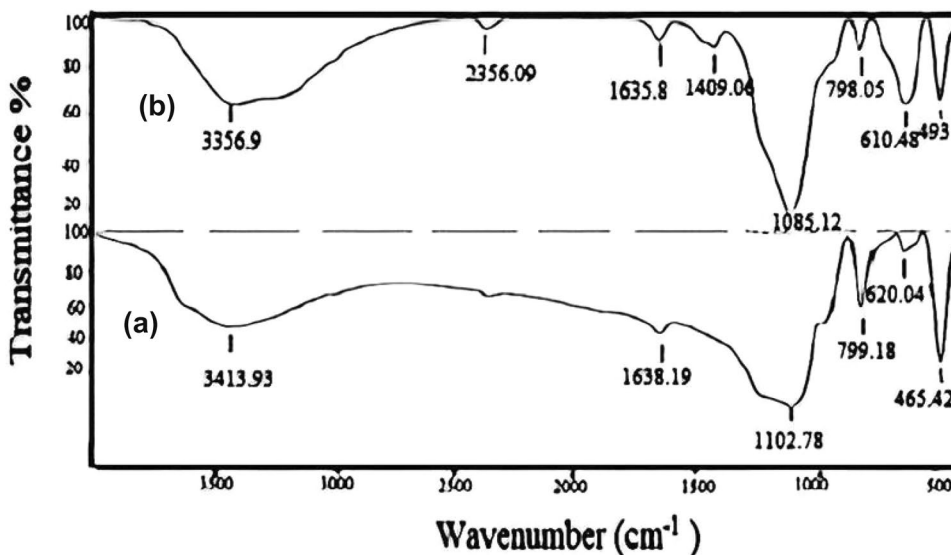


Figure 2 shows the FTIR spectrum of the TZ (a) and the produced MZ nanocomposite (b). The IR absorption bands in the 465, 620, 799, 1102 cm^{-1} range correspond to the TZ. The absorption peak at 465 cm^{-1} and 799 cm^{-1} is related to the bending vibrations of M–O bonds and stretching vibration modes of O–M–O groups (M=Si and Al), respectively [26, 48]. The 1102 cm^{-1} band is related to M–O bonds in MO_4 tetrahedra, which make transition to 1085 cm^{-1} in nanocomposite [26, 48]. The absorption peak at 493 cm^{-1} and 798 cm^{-1} is related to maghemite nanoparticles [24, 39, 42, 44], and this is in agreement with the XRD measurement. The absorption bands at around 610 cm^{-1} are attributed to the Fe–Si–O groups of reacted nanoparticles with zeolite [26]. The absorption bands visible on the spectra around 1638 cm^{-1} are characteristic of vibrations in structural water molecules, and the band at 3413 cm^{-1} is

attributed to –OH-stretching [42–47]. Finally, the tiny dip in the spectra at 2356 cm^{-1} is due to atmospheric CO_2 [39, 42].

Figure 3 is the SEM images of the treated and magnetic zeolite nanocomposite, which shows that most of the zeolite has a smoother surface with morphology of multilayer/single plate, and the maghemite ($\gamma\text{-Fe}_2\text{O}_3$) nanoparticles are spherical, which is located on their surface. Due to the $\gamma\text{-Fe}_2\text{O}_3$ nanoparticles bonded with the TZ surface, the BET surface area decreases from 155 m^2/g for TZ to 102 m^2/g for MZ, and also pore volume decreases from 0.14 cm^3/g in TZ to around 0.093 cm^3/g in MZ. The phenomena could be related to the formation of maghemite nanoparticles inside the pores [43].

Figure 4 is the TEM images of the MZ nanocomposite. The average size of 150 randomly chosen particles was 21 ± 2 nm. This result is in agreement with the XRD

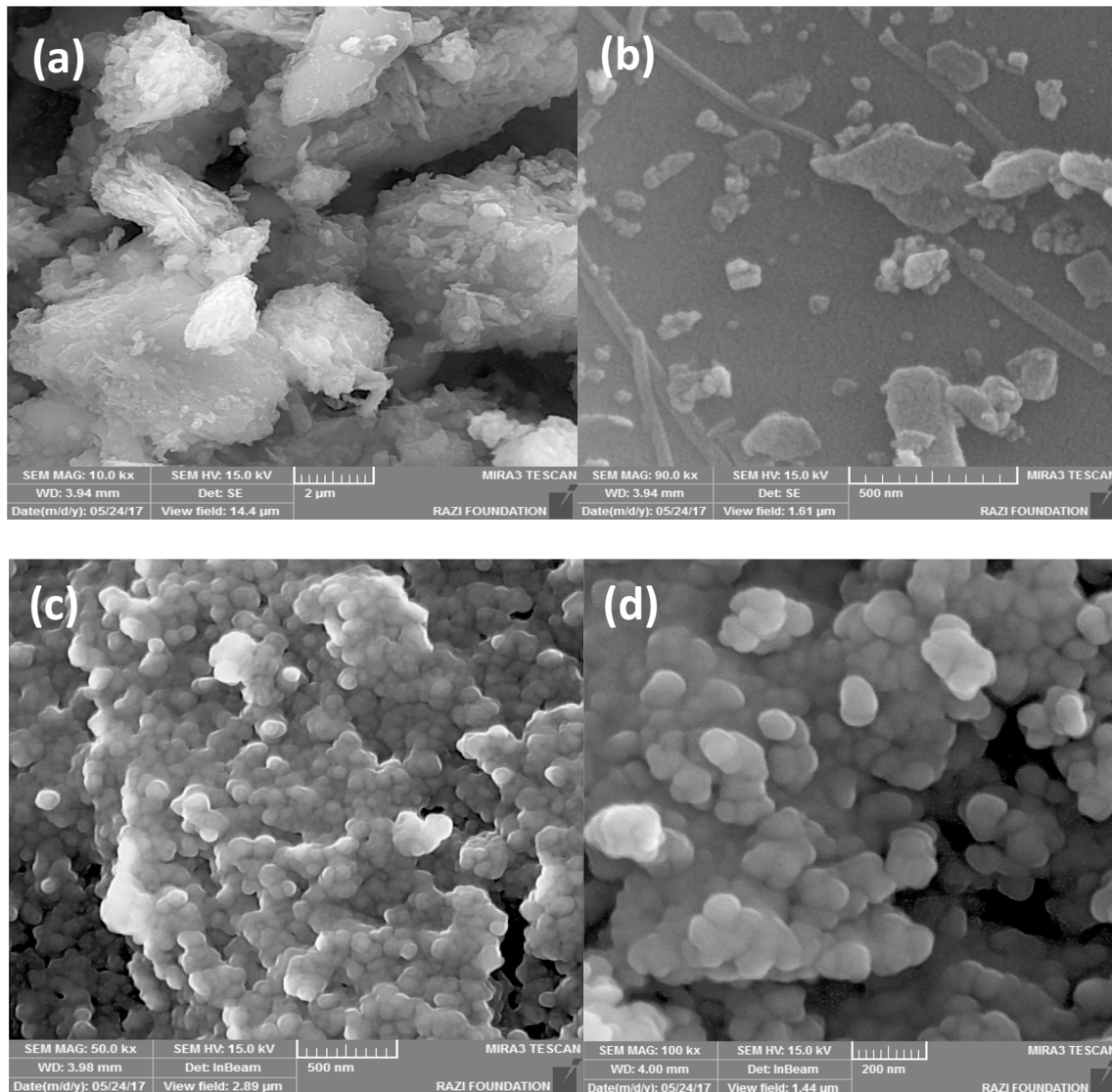


Fig. 3 SEM images of a, b TZ and c, d MZ

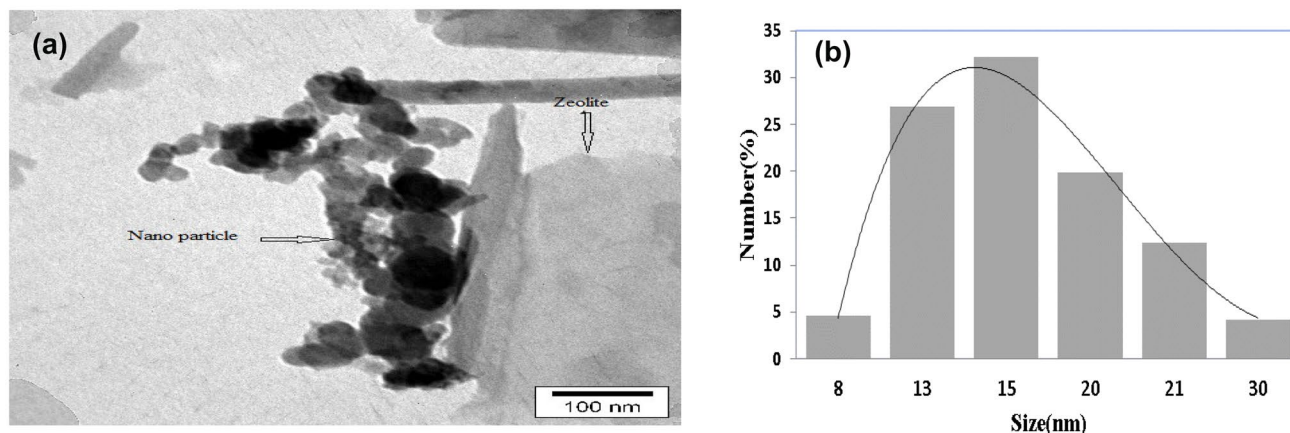
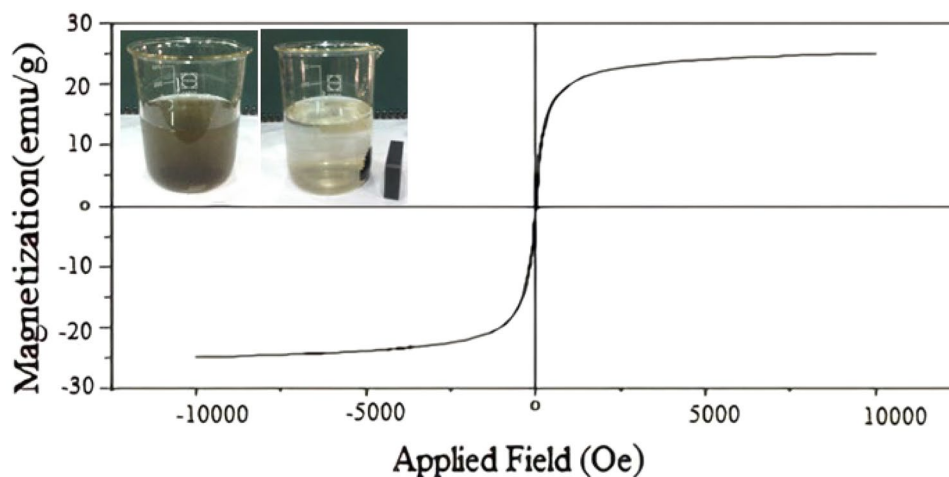


Fig. 4 **a** Typical TEM images of MZ by maghemite nanoparticles (240,000 \times); **b** Particle size distribution for maghemite nanoparticles on MZ

Fig. 5 Magnetic hysteresis curves measured at room temperature for MZ



analysis (~ 18 nm). However, it is evident that maghemite nanoparticles were bonded to the surface of the TZ. The magnetization curves at room temperature plotted against H/T for MZ are shown in Fig. 5. The magnetization saturation occurred at relatively low external field (~ 5000 Gaussian). It indicates a narrow particle-size distribution and a good crystalline of the maghemite nanoparticles. Low magnetic remanence ($M_r = 0.43$) indicated that the produced maghemite nanoparticles are super-paramagnetic at ambient temperature. This observation is consistent with reference [16]. The saturation magnetization was $23.5 \text{ A m}^2 \text{ kg}^{-1}$ (emu/g) for MZ; the value for bulk $\gamma\text{-Fe}_2\text{O}_3$ crystallites is $73.5 \text{ A m}^2 \text{ kg}^{-1}$, where the difference is due to the surface spin canting and disorder broken bonds, whose effect becomes increasingly important with decreasing particle size. Moreover, MZ could be quickly separated from the solution and brought to the side wall of a cuvette within 10 s using an ordinary magnet

(insert Fig. 5), suggesting that MZ had excellent magnetic properties.

The pH_{ZPC} of MZ nanocomposite produced in this study by the chemical precipitation method was approximately 6.8. For the pH higher and lower than ZPC, the surface of nanocomposite contains negative and positive charges attracting cations and anions, respectively (by electrostatic forces), while at this point, the positive charges equal the negative ones [32, 39, 43].

Adsorption tests

Effect of pH

Figure 6a depicts NO_3^- adsorption on the MZ at 25°C during 48 h with different initial pH values. The results demonstrated that NO_3^- adsorption in acidic pH range (3 to 6) is higher while at alkaline pH (greater than 7), nitrate

Fig. 6 a Effect of pH on the adsorption of nitrate ions by MZ and **b** diagram of the fractional-pH for the nitrate-water system at 25 °C. (Drawn by Medusa software, Royal Institute of Technology, Sweden)

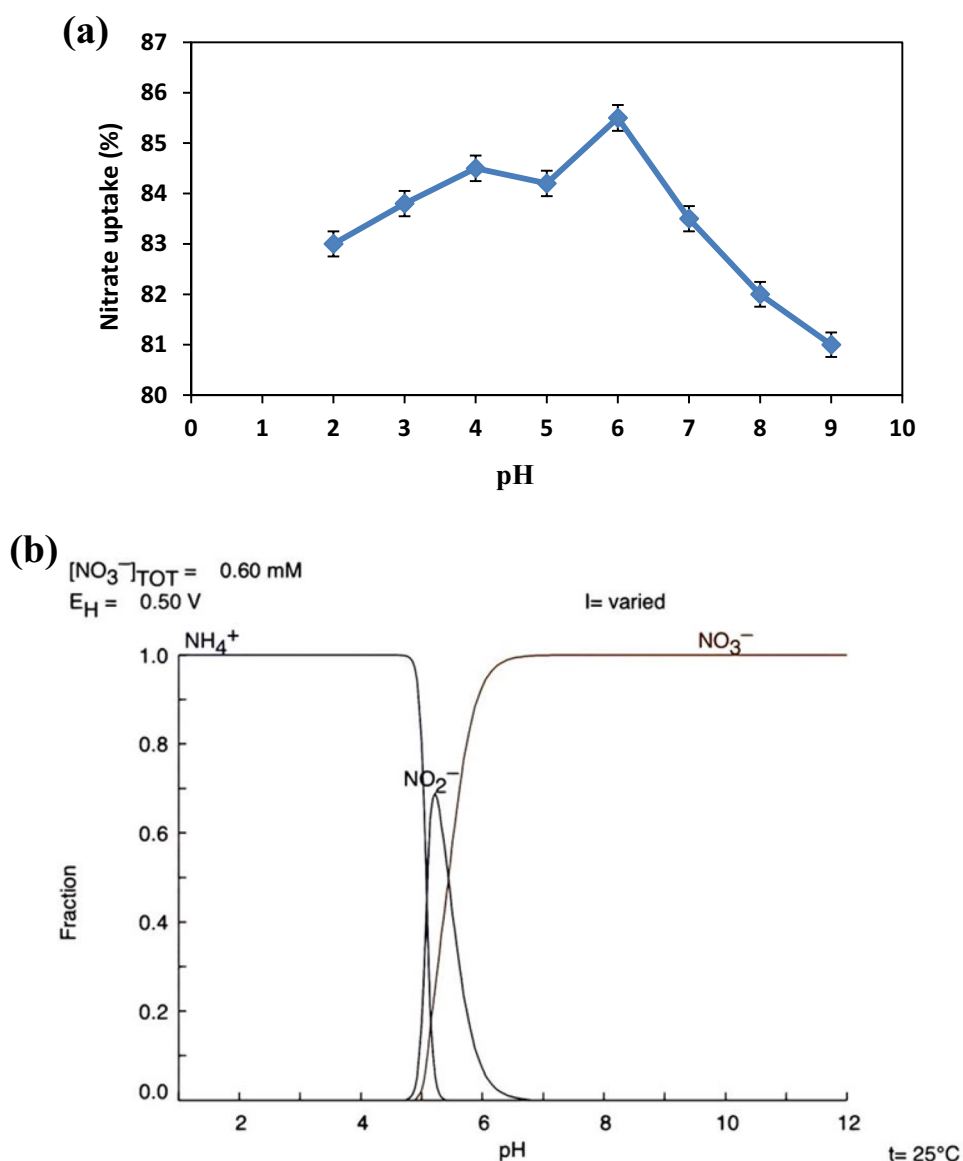


Table 1 Logarithms of association constants for nitrate complexes [32]

Reaction	Log K (25 °C)
$10\text{H}^+ + \text{NO}_3^- + 8\text{e}^- \rightarrow \text{NH}_4^+ + 3\text{H}_2\text{O}$	119.137
$8\text{H}^+ + \text{NO}_3^- + 6\text{e}^- \rightleftharpoons \text{NH}_3\text{OH}^+ + 2\text{H}_2\text{O}$	73.62
$17\text{H}^+ + 2\text{NO}_3^- + 14\text{e}^- \rightleftharpoons \text{N}_2\text{H}_5^+ + 6\text{H}_2\text{O}$	196.04
$2\text{H}^+ + \text{NO}_3^- + 2\text{e}^- \rightleftharpoons \text{NO}_2^- + \text{H}_2\text{O}$	27.78
$8\text{H}^+ + 2\text{NO}_3^- + 8\text{e}^- \rightleftharpoons \text{N}_2\text{O}_2^- + 4\text{H}_2\text{O}$	101.33
$\text{H}_2\text{O} \rightleftharpoons \text{H}^+ + \text{OH}^-$	-14.002
$2\text{H}_2\text{O} \rightleftharpoons 3\text{H}^+ + \text{HO}_2^- + 2\text{e}^-$	-71.26
$\text{KNO}_3 + \text{H}_2\text{O} \rightleftharpoons \text{K}^+ + \text{NO}_3^- + \text{OH}^- + \text{H}^+$	1.18

adsorption drops. In fact, the increase in the amount of hydroxyl ions in the solution at highly alkaline pH results in a competition between nitrate ions and hydroxyl to occupy active adsorption sites on the MZ, while decreasing NO_3^- adsorption [30]. Also, the nitrate ions in solution were replaced by the hydroxyl (OH^-) ions present in MZ (ion exchange). This observation is consistent with what was reported by reference [15].

Table 1 shows the stability constant logarithm (Log K) related to each stable nitrate species in the pH range of 1–14. According to Log K, the formation of NH_4^+ , NH_3OH^+ , N_2H_5^+ , NO_2^- and N_2O_2^- is possible at acidic pH that can increase or decrease the adsorption ability or kinetics of MZ. According to the diagram of the species obtained by Fig. 6b, the three types of nitrates are formed in solution at different pH, where NO_3^- is converted to NH_4^+ ions at pH lower

Fig. 7 The mechanisms of nitrate adsorption on the zeolite/ γ - Fe_2O_3 nanocomposite

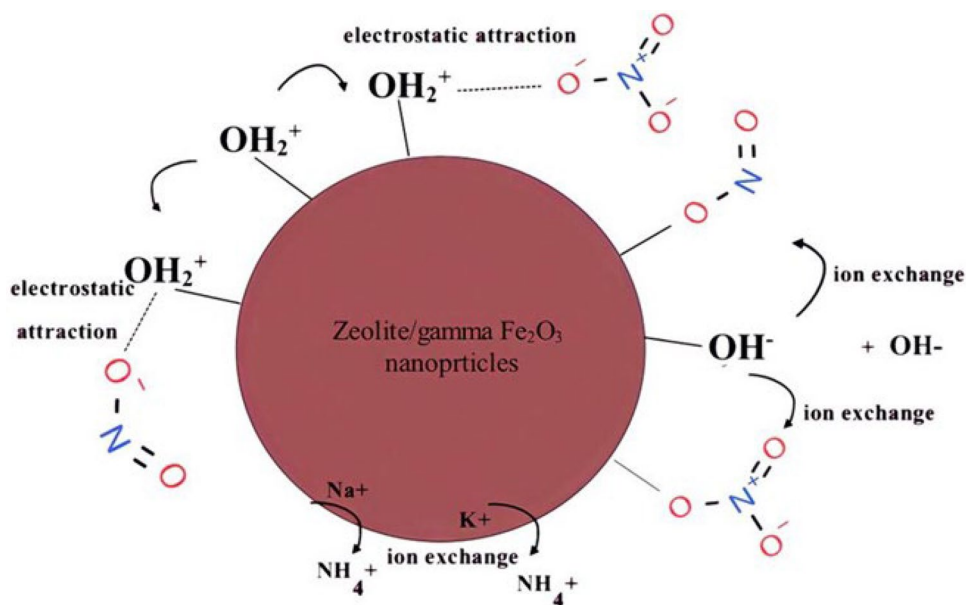
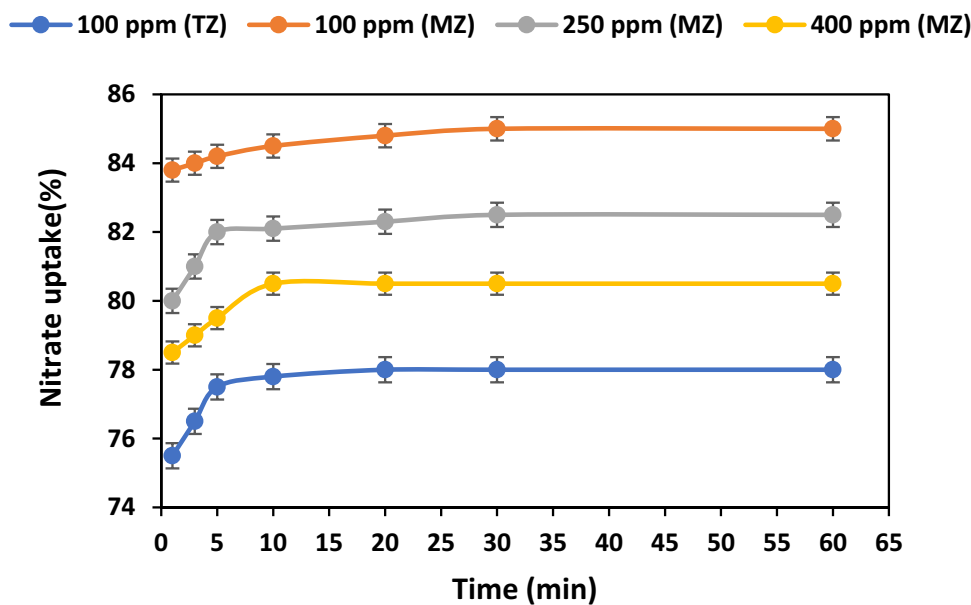


Fig. 8 Effect of initial concentration and contact time on the adsorption of nitrate removed by TZ, and MZ; dosage of adsorbent 0.2 g/L at ambient temperature



than 4. Therefore, it is postulated that NH_4^+ was removed by ion exchanges with Na^+ and K^+ in zeolite structure. Additionally, the proposed mechanisms for nitrate adsorption on nanocomposite surface are shown in Fig. 7.

Effect of contact time and initial concentration

The effect of initial nitrate concentrations and contact time on the removal by TZ and MZ is shown in Fig. 8. The removal percentages for MZ with respect to initial concentrations reveal approximately 5 min to approach steady state. After this time, the removal percentages of nitrate are 84.2, 82, and 79.5 for initial concentration of 100, 250,

and 400 g/L, respectively. So, by increasing the nitrate concentration from 100 to 400 mg/L, the removal of nitrate decreases by only 4.7 percent (high to low difference) and the time required to reach equilibrium slightly increases. Therefore, for low nitrate concentrations, the empty space within the adsorbent is large enough, while increasing the nitrate concentration causes suitable spaces to be filled up first. Then, the amount of residual nitrate moves from the bulk solution toward the adsorbent and hardly penetrates into the pores and adsorbs within the empty space of the adsorbent. This mass transfer resistance increases the adsorption time.

The three concentrations of nitrate after removal have decreased from 100 to 16.5 mg/L, 250 to 45 mg/L, and 400 to 75 mg/L. According to WHO, the maximum levels of nitrate in drinking water are 50 mg/L [1]. Therefore, concentrations of 100 and 250 mg/L reach below the allowable limit after removal.

In addition, 77.5% of nitrate removal occurred by a dosage of 0.2 g/L TZ and at 100 mg/L initial nitrate concentration. The results showed that the removal of nitrate

(100 mg/L initial concentration) with the MZ was only 6.7% higher than that of the TZ, but its separation from solution by a manual magnet was advantageous with respect to cost and time compared to filtration and centrifugation methods used for conventional zeolite.

Fig. 9 Effect of adsorbent dosage on percentage removal of nitrate by MZ

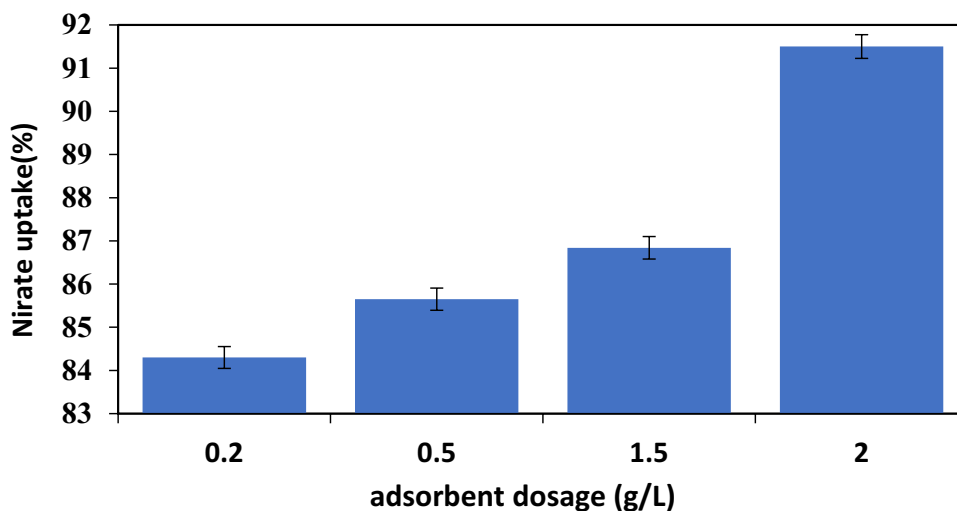


Table 2 Comparison of adsorption capacities and other parameters of nitrate removal between this research and literature

Adsorbent	Exp. adsorption capacity (mg/g)	Nitrate concentration (mg/L)	Time	Temperature (°C)	pH	Adsorption isotherm model	References
Zeolite/gamma Fe ₂ O ₃ nanocomposite	421.5	100	5 min	25	6	Langmuir	This research
Zinc ferrite@activated carbon	75.58	100	120 min	30	7	Langmuir	[6]
Zirconium encapsulated chitosan quaternized	138.4	100	30 min	25	6.6	Langmuir	[4]
Magnetic MWCNTs	112	100	120 min	25	6	Langmuir	[17]
Carbon nanotubes functionalized with mesoporous silica-nitrenium ions (CNT-MS-N)	112	80	5 h	30	7	Langmuir	[18]
Polyaniline-modified activated carbon (PAN/AC)	48.9	75	120 min	25	6.6	Sips model	[19]
AC/Al ₂ O ₃ nanoparticles	300	30	75 min	25	4	–	[3]
Cation exchange resin-supported iron and magnesium oxides/hydroxides composite (Fe–Mg/CER)	200	100	30	40	5	–	[10]
Modified zeolite by surfactant (UZM-5)	18.62	100	12 h	25	6	Langmuir	[21]
Chitosan/Zeolite Y/Nano-ZrO ₂ nanocomposite (CTS/ZY/nano-ZrO ₂)	23.58	20	60 min	35	3	Langmuir	[22]
Amine-modified cocoa shell (ECAB)	31.65	50	180 min	20	5.5	Langmuir and Freundlich	[23]
Mesoporous carbon CMK-3	48.78	50–250	5 min	25	7	Langmuir	[7]
Zeolite-supported zero-valent iron nanoparticles	22.94	100	24 h	25	5.5	Langmuir	[41]
Modified Clinoptilolite zeolite	21.66	100	180 min	25	5	Langmuir	[48]

Table 3 Thermodynamic parameters of nitrate adsorption in concentration 100 mg/L

ΔG° (kJ/mol)			ΔH° (kJ/mol)	ΔS° (J/mol K)	R^2
298 K	308 K	318 K			
-4.152	-4.008	-3.95	-6.015	-6.51	0.9814

Table 4 Langmuir and Freundlich constant for the adsorption of nitrate on MZ

Langmuir constants			Freundlich constants		
q_m (mg/g)	K (L/mg)	R^2	n	K	R^2
500	0.06	0.98	1.8	5.23	0.89

Effect of adsorbent dosage

The effect of *adsorbent dosage* on the removal of nitrate by MZ is shown in Fig. 9. Increasing the amount of MZ from 0.2 to 2 g/L led to increasing the removal amount by about 7.2% (from 84.3 to 91.5), which is not significant. Therefore, the adsorbent concentration of 0.2 g/L was selected as the appropriate dose for the other experiments. Referring to Table 2, which shows a comparison between the results of this study using MZ with other researchers who worked with other adsorbents for nitrate removal, the present study has the highest adsorption capacity (421.5 mg/g) after 5 min at initial nitrate concentration of 100 mg/L with adsorbent dosage of 0.2 g/L at room temperature. The closest result to the current study appearing in reference [7] using mesoporous carbon reports an adsorption capacity of roughly 1/9th of this study at the same residence time.

Calculation of thermodynamic parameters and the effect of temperature

The thermodynamic parameters of nitrate adsorption in concentration of 100 mg/L are produced by the thermodynamic equations as shown in Table 3 and in Fig. S1 (supplementary of materials). A negative value of ΔH° confirms the exothermic nature of nitrate adsorption and proves that

the adsorption increases by decreasing the solution temperature. The obtained ΔG° values for temperatures 298, 308 and 318 K were -4.152, -4.008, and -3.95 kJ/mol, respectively. The low temperatures yield a more negative Gibbs free energy in surface reactions, resulting in a more spontaneous nitrate adsorption process. A negative observed ΔS° was indicative of decreasing disorder, and consequently, increasing adsorption levels in the mutual liquid–solid phase at lower temperatures during the adsorption process [32].

Adsorption isotherm models

Table 4 shows how the isotherm parameters were obtained by fitting the adsorption data with Langmuir and Freundlich models. Based on the high correlation coefficient of the data with the Langmuir model ($R^2=0.98$), it can be concluded that adsorption of nitrate on the MZ is performed as a single layer on the adsorbent surface and there is no interaction between the adsorbed units (Fig. S2). Also, the adsorbent surface is homogeneous and the heat of absorption is uniform. The maximum amount of adsorbed nitrate (q_{max}) was 500 mg/g at 25 °C. The Freundlich isotherm model yielded a 0.89 correlation coefficient (R^2) at ambient temperature (Fig. S3).

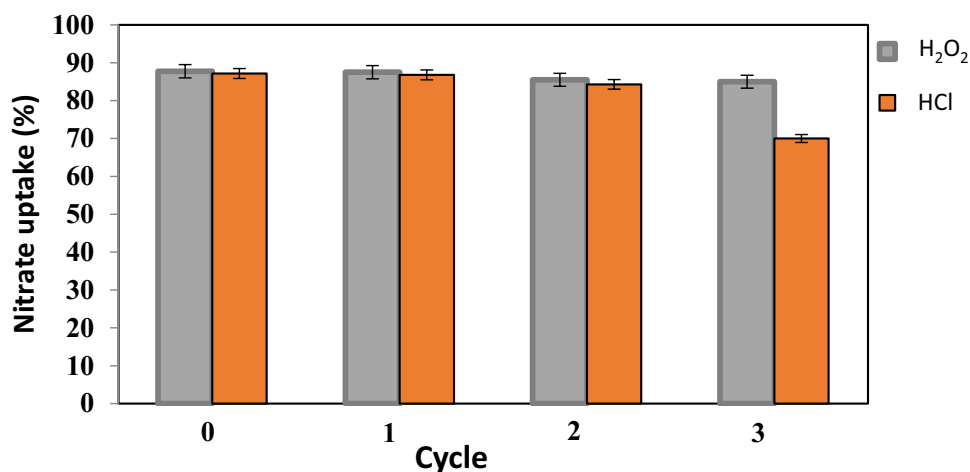
Kinetic study of adsorption

The kinetic parameters of nitrate adsorption by MZ adsorbents are shown in Table 5. In pseudo-first-order kinetics, calculated adsorption capacity ($q_{e,cal}$) does not represent experimental adsorption capacity ($q_{e,exp}$) (Fig. S4). However, the calculated adsorption capacity, in comparison with the experimental adsorption capacity in pseudo-second-order, shows high agreement ($R^2=0.99$), and therefore, nitrate adsorption conforms with pseudo-second-order kinetics (Fig. S5). The reaction expressed by the quasi-quadratic kinetic model is directly proportional to the number of active sites on the adsorbent surface. The pseudo-second-order kinetics model is based on the assumption that the reaction-limiting step may be chemical adsorption. Therefore, the adsorption of nitrate by MZ is a chemical adsorption and not a physical adsorption [6]. These results are consistent with

Table 5 Kinetics parameters for nitrate adsorption on the MZ in the concentration of 0.2 g/L of MZ

Adsorbate dose (mg/L)	Pseudo-second-order Parameters				Pseudo-first-order Parameters		
	K_s (min ⁻¹)	$q_{e,Cal}$ (mg/g)	$q_{e,exp}$ (mg/g)	R^2	K_f (min ⁻¹)	$q_{e,Cal}$ (mg/g)	R^2
100	0.0024	417	421.5	0.998	-0.0338	1.72	0.80
250	0.001	1040	1043.5	0.999	0.0877	2.90	0.89
400	0.0006	1600	1620	0.999	0.0064	2.84	0.67

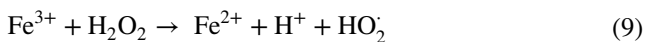
Fig. 10 Adsorption–desorption for MZ nanocomposite on the adsorption percentage of nitrate ions



the results of a study by Pavlovik et al. [48] that examined the nitrate removal with MZ by iron oxide nanoparticles.

Regeneration and reuse

According to Fig. 10, the percentage of nitrate removal by fresh MZ was 87.8%, while after regeneration 1, 2 and 3 times with H₂O₂ solution, the removal percentage was 87.4%, 85.5% and 85%, respectively. After the same number of regenerations by HCl solution, the removal percentages decreased to 86.8%, 84.4% and 70%, respectively, due to the regeneration of the active space on the adsorbent after each adsorption step. According to the diagram of the species shown in Fig. 6b, NH₄⁺ ions formed at pH lower than 4. Therefore, NH₄⁺ was desorbed by ion exchanges with H⁺ in acidic media (HCl) from MZ nanocomposites. Referring to reaction-9 (below) using hydrogen peroxide, since zeolite has been improved by gamma-Fe₂O₃ nanoparticles, there is a tendency to produce H⁺ ions and HO₂[•] radicals [49]. The formation of the ions and radicals improves the elimination of nitrate ions in successive cycles with respect to HCl.



These results indicate better performance of H₂O₂ than HCl in regenerating the adsorbent. They also show that the prepared MZ can be easily regenerated by H₂O₂ and therefore is highly durable.

Conclusion

In comparison with the other adsorbents used for nitrate removal, the present study revealed that the MZ exhibits high adsorption capacity (421.5 mg/g) after 5 min with adsorbent dosage of 0.2 g/L. However, the reference [7]

method using mesoporous carbon produced an adsorption capacity of roughly 1/9th of this study at the same residence time (Table 2). In addition, the highest percentage removal of nitrate was 91.5% at initial nitrate concentration of 100 mg/L, adsorbent dosage of 2 g/L and pH=6. It is also concluded that separation of adsorbent from solution by a manual magnet was advantageous with respect to cost and time compared to filtration and centrifugation methods used for conventional zeolite. Therefore, the MZ is an economical, efficient and effective adsorbent as compared with other reported adsorbents. From the thermodynamic point of view, the increase in nitrate removal was associated with a decrease in enthalpy and entropy. This implies that the exothermic reaction occurs with less disorder which raises the amount of available energy for removal. In addition, the adsorption process of nitrate followed the Langmuir model and pseudo-second-order kinetics. Finally, it is recommended to continue research in substantiating the claim that the formation of H⁺ ions and HO₂[•] radicals by H₂O₂ during the regeneration of adsorbent improves the elimination of nitrate ions.

Supplementary Information The online version contains supplementary material available at <https://doi.org/10.1007/s41204-022-00294-6>.

Acknowledgements The authors thank Dr. Alexander-Eskandar V. Mirzamoghadam, a native USA English speaker who is also affiliated with Shahid Bahonar University of Kerman as professor in the college of Engineering for reviewing, editing, and offering excellent suggestions to improve the manuscript.

Declaration

Conflict of interest The authors declare that they have no known conflict of interests or personal relationships that could have appeared to influence the work reported in this paper.

References

- Keshvardoostchokami M, Majidi M, Zamani A, Liu B (2021) A review on the use of chitosan and chitosan derivatives as the bio-adsorbents for the water treatment: removal of nitrogen-containing pollutants. *Carbohydr Polym* 273:118625–118637. <https://doi.org/10.1016/j.carbpol.2021.118625>
- Bhatnagar A, Sillanpää M (2011) A review of emerging adsorbents for nitrate removal from water. *Chem Eng J* 168:493–504. <https://doi.org/10.1016/j.cej.2011.01.103>
- Velu M, Balasubramanian B, Velmurugan P, Kamyab H, Ravi AV, Chelliapan S, Lee CT, Palaniyappan J (2021) Fabrication of nanocomposites mediated from aluminium nanoparticles/Moringa oleifera gum activated carbon for effective photocatalytic removal of nitrate and phosphate in aqueous solution. *J Clean Prod* 281:124553. <https://doi.org/10.1016/j.jclepro.2020.124553>
- Banu HAT, Karthikeyan P, Meenakshi S (2021) Removal of nitrate and phosphate ions from aqueous solution using zirconium encapsulated chitosan quaternized beads: Preparation, characterization and mechanistic performance. *Results Surfaces Interfaces* 3:100010–100020. <https://doi.org/10.1016/j.rsufri.2021.100010>
- Gomaa HE, Alotaibi AA, Gomaa FA, Bajuayfir E, Ahmad A, Alotaibi KM (2021) Integrated ion exchange-based system for nitrate and sulfate removal from water of different matrices: analysis and optimization using response surface methodology and Taguchi experimental design techniques. *Process Saf Environ Prot* 153:500–517. <https://doi.org/10.1016/j.psep.2021.07.045>
- Karthikeyan P, Sirajudheen P, Nikitha MR, Meenakshi S (2020) Removal of phosphate and nitrate via a zinc ferrite@activated carbon hybrid composite under batch experiments: study of isotherm and kinetic equilibriums. *Environ Nanotechnol Monit Manag* 14:100378–100387. <https://doi.org/10.1016/j.enmm.2020.100378>
- Kiomarsipour N, Alizadeh M, Alizadeh M, Ghani K (2021) Synthesis and surface-functionalizing of ordered mesoporous carbon CMK-3 for removal of nitrate from aqueous solution as an effective adsorbent. *Diam Relat Mater* 116:108419–108430. <https://doi.org/10.1016/j.diamond.2021.108419>
- Ferro S (2012) Removal of nitrates from highly-contaminated industrial wastewater. *Crit Rev* 12:101–110
- Dey S, Haripavan N, Basha SR, Babu GV (2021) Removal of ammonia and nitrates from contaminated water by using solid waste bio-adsorbents. *Curr Res Chem Biol* 1:100005–100020. <https://doi.org/10.1016/j.crchbi.2021.100005>
- Nguyen TT, Tran VAK, Tran LB, Phan PT, Nguyen MT, Bach LG, Padungthon S, Ta CK, Nguyen NH (2021) Synthesis of cation exchange resin-supported iron and magnesium oxides/hydroxides composite for nitrate removal in water. *Chin J Chem Eng* 32:378–384. <https://doi.org/10.1016/j.cjche.2020.11.032>
- Lau YL, Yeong YF (2016) Optimization of nitrate removal from aqueous solution by amine-functionalized MCM-41 using response surface methodology. *Procedia Eng* 148:1239–1246. <https://doi.org/10.1016/j.proeng.2016.06.485>
- Abu A, Abdullah N (2021) Sorption and thermodynamic study of nitrate removal by using Amberlite IRA 900 (AI900) resin. *Mater Today: Proc* 41:102–108. <https://doi.org/10.1016/j.matpr.2020.11.1014>
- Dong H, Shepsko CS, German M, SenGupta AK (2020) Hybrid nitrate selective resin (NSR-NanoZr) for simultaneous selective removal of nitrate and phosphate (or fluoride) from impaired water sources. *J Environ Chem Eng* 8:1. <https://doi.org/10.1016/j.jece.2020.103846>
- Song N, Xu J, Cao Y, Xia F, Zhai J, Ai H, Shi D, Gu L, He Q (2020) Chemical removal and selectivity reduction of nitrate from water by (nano) zero-valent iron/activated carbon micro-electrolysis. *Chemosphere* 248:125986–125997. <https://doi.org/10.1016/j.chemosphere.2020.125986>
- Liu Y, Zhang X, Wang J (2022) A critical review of various adsorbents for selective removal of nitrate from water: structure, performance and mechanism. *Chemosphere* 291:132728–132750. <https://doi.org/10.1016/j.chemosphere.2021.132728>
- Palko JW, Oyarzun DI, Ha B, Stadermann M, Santiago JG (2018) Nitrate removal from water using electrostatic regeneration of functionalized adsorbent. *Chem Eng J* 334:1289–1296. <https://doi.org/10.1016/j.cej.2017.10.161>
- Lee H-K, Yoo D-H, Jo S-E, Choi S-J (2021) Removal of nitrate from radioactive wastewater using magnetic multi-walled carbon nanotubes. *Prog Nucl Energy* 140:103893–103900. <https://doi.org/10.1016/j.pnucene.2021.103893>
- Ahmad R, Ansari K (2022) Novel in-situ fabrication of L-methionine functionalized bionano-composite for adsorption of Amido Black 10B dye. *Process Biochem* 119:48–57. <https://doi.org/10.1016/j.procbio.2022.05.015>
- Hu Q, Liu H, Zhang Z, Xie Y (2020) Nitrate removal from aqueous solution using polyaniline modified activated carbon: optimization and characterization. *J Mol Liq* 309:113057–113067. <https://doi.org/10.1016/j.molliq.2020.113057>
- Plata-Gryl M, Momotko M, Makowicz S, Boczkaj G (2022) Characterization of diatomaceous earth coated with nitrated asphaltene as superior adsorbent for removal of VOCs from gas phase in fixed bed column. *Chem Eng J* 427:130653–130666. <https://doi.org/10.1016/j.cej.2021.130653>
- Aghai MD, Pakizeh M, Ahmadpour A (2013) Synthesis and characterization of modified UZM-5 as adsorbent for nitrate removal from aqueous solution. *Sep Purif Technol* 113:24–32. <https://doi.org/10.1016/j.seppur.2013.04.013>
- Teimouri A, Nasab SG, Vahdatpoor N, Habibollahi S, Salavati H, Chermahini AN (2016) Chitosan /Zeolite Y/Nano ZrO₂ nanocomposite as an adsorbent for the removal of nitrate from the aqueous solution. *Int J Biol Macromol* 93:254–266. <https://doi.org/10.1016/j.ijbiomac.2016.05.089>
- Nkuigue Fotsing P, Bouazizi N, Djoufack Woumfo E, Mofaddel N, Le Derf F, Vieillard J (2021) Investigation of chromate and nitrate removal by adsorption at the surface of an amine-modified cocoa shell adsorbent. *J Environ Chem Eng* 9:104618–104630. <https://doi.org/10.1016/j.jece.2020.104618>
- Ahmad R, Ansari K, Ejaz MO (2022) Enhanced sequestration of heavy metals from aqueous solution on polyacrylamide grafted with cell@Fe₃O₄ nanocomposite. *Emergent Mater* 12:12701. <https://doi.org/10.1007/s42247-021-00338-8>
- Ollier RP, Cano LA, Sanchez LM, Alvarez VA (2021) Advanced applications of green materials in nitrate, phosphate, and fluoride removal. *Adv Green Mater* 20:423–459
- El-Sherbeeney AM, Soliman SR, AlHammadi AA, Shim JJ, Abukhadra MR (2021) Insight into the CaO green decorated clinoptilolite as an effective adsorbent for nitrate and phosphate ions; equilibrium; kinetic, and safety studies. *Surfaces Interfaces* 27:101568–101580. <https://doi.org/10.1016/j.surfin.2021.101568>
- Lazaratou CV, Vayenas DV, Papoulis D (2020) The role of clays, clay minerals and clay-based materials for nitrate removal from water systems: a review. *Appl Clay Sci* 185:105377–105385. <https://doi.org/10.1016/j.clay.2019.105377>
- Zhang S, Kong Z, Wang H, Yan Q, Vayenas DV, Zhang G (2021) Enhanced nitrate removal by biochar supported nano zero-valent iron (nZVI) at biocathode in bioelectrochemical system (BES). *Chem Eng J* 1:133535–133545. <https://doi.org/10.1016/j.cej.2021.133535>
- Lee J-H, Velmurugan P, Ravi AV, Oh B-T (2020) Green and hydrothermal assembly of reduced graphene oxide (rGO)-coated ZnO and Fe hybrid nanocomposite for the removal of nitrate and

- phosphate. *Environ Chem Ecotoxicol* 2:141–149. <https://doi.org/10.1016/j.enceco.2020.08.001>
30. Loganathan P, Vigneswaran S, Kandasamy J (2013) Enhanced removal of nitrate from water using surface modification of adsorbents—a review. *J Environ Manag* 131:363–374. <https://doi.org/10.1016/j.jenvman.2013.09.034>
 31. El Hanache L, Sundermann L, Lebeau B, Toufaily J, Hamieh T, Daou TJ (2019) Surfactant-modified MFI-type nanozeolites: super-adsorbents for nitrate removal from contaminated water. *Microporous Mesoporous Mater* 283:1–13. <https://doi.org/10.1016/j.micromeso.2019.03.049>
 32. Darezereshki E, Darban AK, Abdollahy M, Jamshidi-Zanjani A (2018) Influence of heavy metals on the adsorption of arsenate by magnetite nanoparticles: Kinetics and thermodynamic. *Environ Nanotechnol Monit Manag* 10:51–62. <https://doi.org/10.1016/j.enmm.2018.04.002>
 33. Imgharn A, Anchoum L, Hsini A, Naciri Y, Laabd M, Mobarak M, Aarab N, Bouziani A, Szunerits S, Boukherroub R, Lakhmiri R, Albourine A (2022) Effectiveness of a novel polyaniline@Fe-ZSM-5 hybrid composite for Orange G dye removal from aqueous media: Experimental study and advanced statistical physics insights. *Chemosphere* 295:133786. <https://doi.org/10.1016/j.chemosphere.2022.133786>
 34. Brini L, H'Maida K, Imgharn A, Hsini A, Naciri Y, Ajmal Z, Bouziani A, Boulahya A, Arahou M, Bakiz B, Albourine A, Fekehaoui M (2021) Synthesis and characterisation of PANI-coated Heliotrope Leaves (PANI@HL) with high clean-up capacity for Orange G dye from aqueous media. *Int J Environ Anal Chem* 2:1994557. <https://doi.org/10.1080/03067319.2021.1994557>
 35. Amjlef A, Khrach S, El Fakir AA, Farsad S, Et-Taleb S, El Alem N (2021) Adsorptive properties investigation of natural sand as adsorbent for methylene blue removal from contaminated water. *Nanotechnol Environ Eng* 26:1–15. <https://doi.org/10.1007/s41204-021-00119-y>
 36. Laabd M, Imgharn A, Hsini A, Naciri Y, Mobarak M, Szunerits S, Boukherroub R, Albourine A (2022) Efficient detoxification of Cr(VI)-containing effluents by sequential adsorption and reduction using a novel cysteine-doped PANi@faujasite composite: experimental study supported by advanced statistical physics prediction. *J Hazard Mater* 422:126857. <https://doi.org/10.1016/j.jhazmat.2021.126857>
 37. Imgharn A, Ighnih H, Hsini A, Naciri Y, Laabd M, Kabli H, Elamine M, Lakhmiri R, Souhail B, Albourine A (2021) Synthesis and characterization of polyaniline-based biocomposites and their application for effective removal of Orange G dye using adsorption in dynamic regime. *Chem Phys Lett* 778:138811. <https://doi.org/10.1016/j.cplett.2021.138811>
 38. Azari A, Hossein Mahvi A, Naseri S, Rezaei Kalantary R, Saberi M (2014) Nitrate removal from aqueous solution by using modified clinoptilolite zeolite. *Arch Hygiene Sci* 3:184–192
 39. Darezereshki E (2010) Synthesis of maghemite ($\gamma\text{-Fe}_2\text{O}_3$) nanoparticles by wet chemical method at room temperature. *Mater Lett* 64:1471–1472. <https://doi.org/10.1016/j.matlet.2010.03.064>
 40. Darezereshki E, Ranjbar M, Bakhtiari F (2010) One-step synthesis of maghemite ($\gamma\text{-Fe}_2\text{O}_3$) nano-particles by wet chemical method. *J Alloys Compd* 502:257–260. <https://doi.org/10.1016/j.jallcom.2010.04.163>
 41. Sepehri S, Heidarpour M, Abedi-Koupai J (2014) Nitrate removal from aqueous solution using natural zeolite-supported zero-valent iron nanoparticles. *Soil Water Res* 9:224–232
 42. Darezereshki E (2011) One-step synthesis of hematite ($\alpha\text{-Fe}_2\text{O}_3$) nano-particles by direct thermal-decomposition of maghemite. *Mater Lett* 65:642–645. <https://doi.org/10.1016/j.matlet.2010.11.030>
 43. Darezereshki E, Bakhtiari F, Alizadeh M, Behradvakylabad A, Ranjbar M (2012) Direct thermal decomposition synthesis and characterization of hematite ($\alpha\text{-Fe}_2\text{O}_3$) nanoparticles. *Mater Sci Semicond Process* 15:91–97. <https://doi.org/10.1016/j.mssp.2011.09.009>
 44. Darezereshki E, Bakhtiari F, Vakylabad AB, Hassani Z (2013) Single-step synthesis of activated carbon/ $\gamma\text{-Fe}_2\text{O}_3$ nano-composite at room temperature. *Mater Sci Semicond Process* 16:221–225. <https://doi.org/10.1016/j.mssp.2012.08.007>
 45. Akhbarizadeh R, Shayestefar MR, Darezereshki E (2013) Competitive removal of metals from wastewater by maghemite nanoparticles: a Comparison Between Simulated Wastewater and AMD. *Mine Water Environ* 33:89–96. <https://doi.org/10.1007/s10230-013-0255-3>
 46. Darezereshki E, Tavakoli F, Bakhtiari F, Vakylabad AB, Ranjbar M (2014) Innovative impregnation process for production of $\gamma\text{-Fe}_2\text{O}_3$ -activated carbon nanocomposite. *Mater Sci Semicond Process* 27:56–62. <https://doi.org/10.1016/j.mssp.2014.05.049>
 47. Ahmadi A, Heidarzadeh S, Mokhtari AR, Darezereshki E, Harouni HA (2014) Optimization of heavy metal removal from aqueous solutions by maghemite ($\gamma\text{-Fe}_2\text{O}_3$) nanoparticles using response surface methodology. *J Geochem Explor* 147:151–158. <https://doi.org/10.1016/j.gexplo.2014.10.005>
 48. Pavlovic JB, Milenkovic JK, Rajic NZ (2014) Modification of natural clinoptilolite for nitrate removal from aqueous media. *J Serb Chem Soc* 79:1309–1322
 49. Yeh C, Hsu C-Y, Chiu C-H, Huang K-L (2008) Reaction efficiencies and rate constants for the goethite-catalyzed Fenton-like reaction of NAPL-form aromatic hydrocarbons and chloroethylenes. *J Hazard Mater* 151(2):562–569

Publisher's Note Springer Nature remains neutral with regard to jurisdictional claims in published maps and institutional affiliations.

Springer Nature or its licensor holds exclusive rights to this article under a publishing agreement with the author(s) or other rightsholder(s); author self-archiving of the accepted manuscript version of this article is solely governed by the terms of such publishing agreement and applicable law.